How to cite: *Angew. Chem. Int. Ed.* **2022,** *61,* e202205922
International Edition: doi.org/10.1002/anie.202205922
German Edition: doi.org/10.1002/ange.202205922

Nitrogen Fixation

Photoelectrochemical Conversion of Dinitrogen to Benzonitrile: Selectivity Control by Electrophile- versus Proton-Coupled Electron Transfer

Maximilian Fritz, Severine Rupp, Ciara I. Kiene, Sesha Kisan, Joshua Telser, Christian Würtele, Vera Krewald, and Sven Schneider**

Abstract: Nitride complexes are key species in homogeneous nitrogen fixation to NH_3 via stepwise proton-coupled electron transfer (PCET). In contrast, direct generation of nitrogenous organic products from N_2-derived nitrides requires new strategies to enable efficient reductive nitride transfer in the presence of organic electrophiles. We here present a 2-step protocol for the conversion of dinitrogen to benzonitrile. Photoelectrochemical, reductive N_2 splitting produces a rhenium(V) nitride with unfavorable PCET thermochemistry towards ammonia generation. However, *N*-benzoylation stabilizes subsequent reduction as a basis for selective nitrogen transfer in the presence of the organic electrophile and Brønsted acid at mild reduction potentials. This work offers a new strategy for photoelectrosynthetic nitrogen fixation beyond ammonia—to yield nitrogenous organic products.

Introduction

Proton-coupled electron transfer (PCET) is a key concept for the design of efficient redox catalysts.[1] As a prominent example, Nishibayashi reported that Mo pincer catalysts generate over 4000 eq. of NH_3 in the nitrogen reduction reaction (NRR) at ambient conditions with the model PCET reductant SmI_2/H_2O.[2] In fact, most homogeneous NRR catalysts are anticipated to operate via initial PCET to metal-coordinated N_2 as a thermochemically challenging step.[3] An alternative, Haber–Bosch-like pathway that has been considered commences with full N_2 splitting prior to N–H bond formation.[4,5] However, terminal nitride complexes that result from reductive N_2 splitting generally exhibit low to moderate hydrogen atom affinities. This is expressed by N–H bond dissociation free energies ($BDFE_{N-H}$) of the corresponding parent imides that are typically below $\approx$45 kcal mol^{-1} (Scheme 1a).[6] In consequence, the first PCET step after N_2 splitting defines a thermochemical bottleneck for ammonia-selective nitrogen reduction *vs.* competing H_2 evolution.[7] PCET-based strategies will be key to establish efficient, photo- and electro-

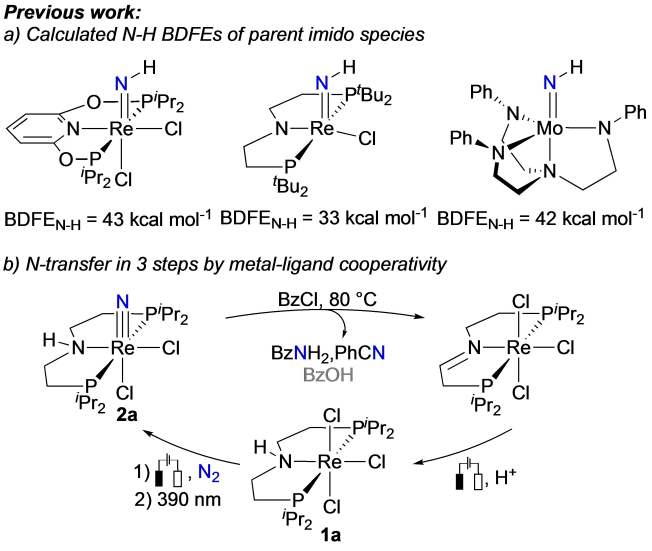

Scheme 1. Computed $BDFE_{N-H}$ for imido complexes relevant to N_2 splitting and PCET-based strategies for selectivity control.

[*] Dr. M. Fritz, C. I. Kiene, S. Kisan, Dr. C. Würtele, Prof. Dr. S. Schneider
Institut für Anorganische Chemie,
Georg August Universität Göttingen
Tammannstraße 4, 37077 Göttingen (Germany)
E-mail: sven.schneider@chemie.uni-goettingen.de
S. Rupp, Prof. Dr. V. Krewald
Theoretische Chemie, Technische Universität Darmstadt
Alarich-Weiss-Straße 4, 64287 Darmstadt (Germany)
E-mail: krewald@chemie.tu-darmstadt.de
Prof. Dr. J. Telser
Department of Biological, Physical and Health Sciences,
Roosevelt University
430 S. Michigan Avenue, Chicago, IL 60605 (USA)

chemically driven NRR catalysis that does not rely on sacrificial chemical reductants.[8]

N_2 splitting also provides a potential entry towards nitrogenous products beyond ammonia. This was demonstrated by several stoichiometric (cyclic) reaction sequences,[5,9] as well as the catalytic formation of trisilylamines and recently triborylamines,[10] directly from N_2. However, several challenges remain to be addressed to obtain more complex targets, like primary amines or amides. For example, electrolysis of a Mo^{IV} alkylimide complex in acidic solution (AcOH) required potentials that are incompatible with most organic electrophiles (−2.3 V vs. $Fc^{+/0}$).[11,12] One-pot or even catalytic product formation via reductive N_2 splitting in the presence of both electrophiles and Brønsted acid necessitates strategies to reduce the overall overpotential and control the N–C vs. N–H bond formation selectivity.

Our groups previously examined N_2 splitting and nitride transfer enabled by (electro-)chemical reduction of rhenium complexes with bulky PNP-pincer ligands.[13] Light-driven N_2 splitting of the modified platform **1a** (Scheme 1b) gave the more reactive nitride **2a**, which converts benzoyl chloride to benzamide upon PCET from the pincer backbone, but only at elevated temperatures.[14] We here present a PCET-based synthetic strategy for direct, cathodic product release in the presence of electrophile and acid. This enabled the development of a one-pot protocol for photoelectrochemical N_2 splitting and benzonitrile formation at mild potentials and ambient temperature (Scheme 1c).

Results and Discussion

We first aimed at replacing BzCl by benzoylation reagents of the higher halides as being better nucleofuge. For that purpose, N_2 splitting with $[ReX_3(^{H}PNP)]$ (**1b**: X = Br, **1c**: X = I; Scheme 2) was examined to avoid complications from halide scrambling during subsequent benzoylation. The bromide and iodide complexes were synthesized from $[ReBr_3(PPh_3)_2(MeCN)]$ and by halide metathesis for **1c**, respectively. Spectroscopic and crystallographic characterization of **1b/c** support rhenium(III) in meridional octahedral coordination.[15] As a typical trend for the halide precursors,[13e,16] cyclic voltammetry (CV) showed that the first reduction of **1b** ($E_{1/2} = -1.70$ V vs. $FeCp_2^{+/0}$)[17] and **1c** ($E_{1/2} = -1.52$ V) are at significantly less negative potentials with respect to **1a** ($E_{1/2} = -1.84$ V).[18] At lower scan rate, the $Re^{III/II}$ couple becomes irreversible for all three halides, which is attributed to X^- loss from $[ReX_3(^{H}PNP)]^-$ as a prerequisite to N_2 activation. Scan rate dependent data allowed for estimating first order halide dissociation rate constants. The increase by almost two orders of magnitude along the halide series ($k_{diss} = 0.05\ s^{-1}$ (**1a**), $0.33\ s^{-1}$ (**1b**), $1.97\ s^{-1}$ (**1c**); Figures S67–S69) correlates with increasing halide ionic radii and polarizability, *viz* leaving group properties.[19,20] Accordingly, the higher halides allowed for photoelectrochemical N_2 splitting by controlled potential electrolysis (CPE) at less negative potentials (Scheme 2).[13e] Furthermore, the productive photolysis window favourably extends further into the visible range. CPE of the halide series ($E_{app} = -1.73$ V (**1b**), −1.53 V (**1c**)) under N_2 with irradiation by a blue LED ($\lambda = 456 \pm 10$ nm) gave increased yields of the nitride complexes **2b** (37 %; Faradaic Efficiency (FE) = 22 %) and **2c** (53 %; FE = 53 %) with respect to the parent chloride (**1b**). Complexes **2b** and **2c** were fully characterized, including crystallography (Figures S98 and S99),[15] which confirmed *cis*-configurations in the solid state as was found for **2a**.[14]

In contrast to **2a**/PhC(O)Cl, benzoylimide formation is directly observed upon addition of excess PhC(O)Br to **2b** in THF. Crystallization gave [Re(NBz)(*H*PNP)]Br (**3^{Br}**) in high yield (Scheme 3). While isolated **3^{Br}** is stable in CH_2Cl_2 over several days, re-dissolving in THF leads to rapid dissociation of benzoyl bromide and a small equilibrium constant was obtained in a titration experiment monitored by ^{31}P NMR spectroscopy ($K_{THF} = 1.1 \times 10^{-5}\ M^{-1}$; Figure S31). However, benzoylimide formation can be driven by halide exchange with $NaBAr^F{}_{24}$ ($BAr^F{}_{24}^- = B\{3,5\text{-}(CF_3)_2C_6H_3\}_4^-$), giving **3^{BArF}** in 90 % yield (Scheme 3). In the solid state, the rhenium(V) benzoyl imido complexes **3^{Br}** and **3^{BArF}** (Figure 1 and Figure S101) exhibit a structural reorganization with respect to the parent nitride **2b** (see above). The *trans*-dibromide configuration of the cation of **3^{Br}** and **3^{BArF}** reflects the decreased *trans*-influence of the multiply bonded nitrogen ligand, as expressed by the significantly longer Re–N multiple bond length (**3^{Br}**: 1.724(3) Å (exp), 1.734 Å (DFT); **2b**: 1.663(5) Å (exp), 1.677 Å (DFT); Table S3/S5). ^1H NOESY characterization (Figure S30/S37) confirmed the *trans* configuration also in

Complex	X	$E_{appl.}$	Wavelength	Yield (FE)
1a	Cl	-1.90 V (1.13 e$^-$ / Re)	390 nm	20% (18%) (**2a**)
1b	Br	-1.73 V (1.70 e$^-$ / Re)	456 nm	37% (22%) (**2b**)
1c	I	-1.53 V (1.0 e$^-$ / Re)	456 nm	53% (53%) (**2c**)

Scheme 2. Photoelectroreductive N_2 splitting with precursors **1a–c** (FE = Faradaic Efficiency).

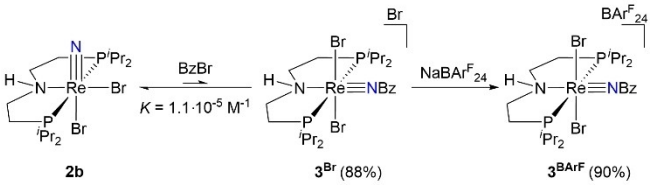

Scheme 3. Benzoylation equilibrium of **2b** and benzoyl bromide.

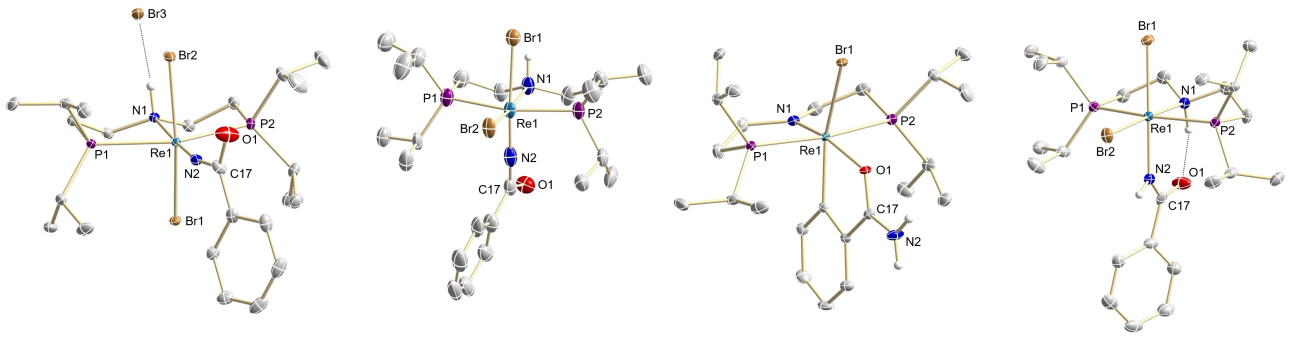

Figure 1. Molecular structures of $\mathbf{3}^{Br}$, **4**, **5** and **6** in the solid state drawn at the 50% probability level. Hydrogen atoms except N–H are omitted for clarity. Selected bond lengths [Å] and angles [°]: $\mathbf{3}^{Br}$: N1-Re1 2.278(3), Re1-N2 1.724(3), N2-C17 1.425(4), C17-O1 1.206(4); Br1-Re1-Br2 165.462(12), N1-Re1-N2 176.37(12). **4**: N1-Re1 2.168(7), Re1-N2 1.788(8), N2-C17 1.343(12), C17-O1 1.251(10); N1-Re1-Br1 170.9(2), Br2-Re1-N2 170.3, P1-Re1-P2 163.70(8). **5**: N1-Re1 1.901(2), N2-C23 1.325(4), C23-O1 1.275(4); Br1-Re1-C17109.35(8), N1-Re1-O1 166.92(9), P1-Re1-P2 166.1481). **6**: N1-Re1 2.161(5), Re1-N2 2.113(4), N2-C17 1.289(7), C17-O1 1.259(7); N1-Re1-Br2 177.47(13), Br1-Re1-N2 176.63(12), P1-Re1-P2 163.19(5).

solution and computations favoured *trans*-$\mathbf{3}^{+}$ over the *cis* isomer by $\Delta G^{0}_{DFT} = 3.8$ kcal mol^{-1}.

Starting from $\mathbf{3}^{+}$, reduction was examined first in the absence of acid. The CV of $\mathbf{3}^{BArF}$ in THF shows a reversible reduction at $E_{1/2} = -0.71$ V ($v = 1.0$ V s^{-1}; Scheme 4) and a reduction at $E_{p,c} = -1.63$ V ($v = 0.1$ V s^{-1}), which was irreversible at all scan rates (Figure S61). Notably, at lower scan rates, the first reduction also becomes increasingly irreversible and a new feature at $E_{p,a} = -0.42$ V grows in the reverse oxidative scan, while the ratio of the cathodic and the sum of the anodic peak currents stays close to unity (Figure S62). These observations are in line with an *ECE* mechanism, namely a chemical step that follows reduction within the CV timescale, which can be attributed to *trans* to *cis* isomerization (see below). Chemical reduction of $\mathbf{3}^{BArF}$ with cobaltocene enabled the isolation of the rhenium(IV) benzoylimido complex [Re(NBz)Br$_2$(*H*PNP)] (**4**) in 85% yield (Scheme 4). Notably, only five-coordinate Re^{IV} oxo and imido complexes were previously reported,[21] and Re^{IV} oxo species have been proposed as reactive intermediates in C–H activation.[22]

The X-band EPR signal of **4** in toluene at room temperature exhibits large ^{187}Re hyperfine interaction ($g = 1.92$, $a_{iso} = 700$ MHz; Figure S40), supporting a low-spin Re^{IV} complex.[23] Structural characterization in the solid state (Figure 1) indicates isomerization to the *cis*-dibromide configuration. Comparison of the molecular structures of $\mathbf{3}^{+}$ and **4** shows a significant elongation of the Re=N bond by 0.09 Å upon reduction despite reduced *trans*-influence in the *cis*-configuration. Isolated **4** exhibits a reversible oxidation at $E_{1/2} = -0.48$ V (Figure S64). We therefore attribute the *ECE* signature of the reduction of $\mathbf{3}^{+}$ to slow isomerization of *trans*-**4** to *cis*-**4** with an estimated rate constant of $k_{iso} \approx 0.04$ s^{-1} (Figure S70). The potential shift ($\Delta E_{1/2} = 0.23$ V; $\Delta\Delta G^{\circ} = 5.3$ kcal mol^{-1}) arises from the difference between the *cis*/*trans*-isomerization equilibria in the oxidized (*cis*/*trans*-$\mathbf{3}^{+}$) and reduced (*cis*/*trans*-**4**) states, respectively, which is well reproduced by DFT ($\Delta\Delta G^{\circ}_{DFT} = 6.7$ kcal mol^{-1}, Figure S94). Isomerization of *trans*-**4** to the more stable *cis*-

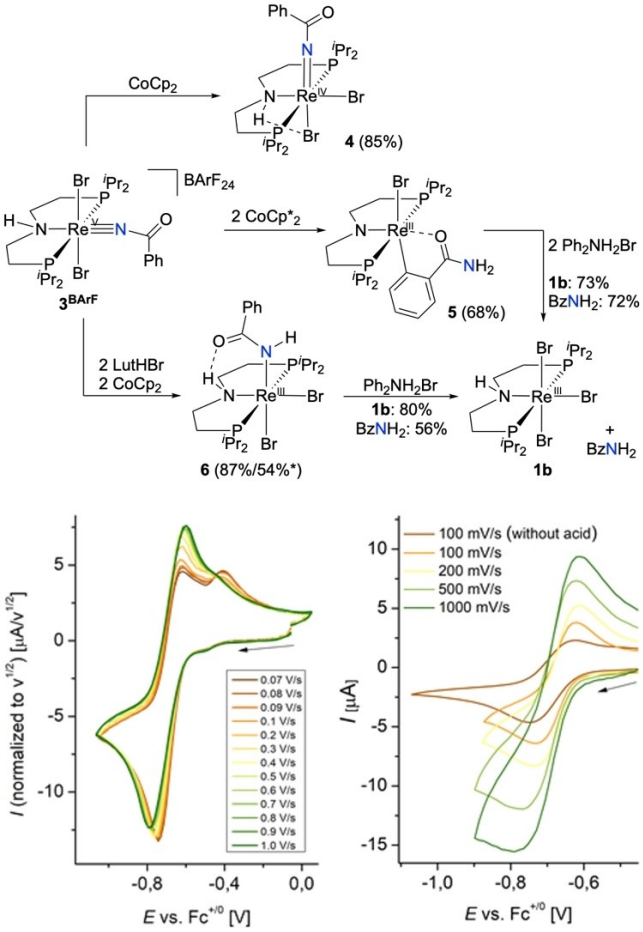

Scheme 4. Top: Synthesis of **4**, **5**, and **6** by reduction of $\mathbf{3}^{BArF}$ including protonolysis of **5** and **6** obtaining **1b** and benzamide. Bottom left: Cyclic voltammetry of the Re$^{V/IV}$ couple of $\mathbf{3}^{BArF}$ (1 mM in THF, 0.1 M N^{n}Bu$_4$PF$_6$) at varied scan rate (currents are normalized to v$^{1/2}$). Bottom right: Cyclic voltammetry of $\mathbf{3}^{BArF}$ in presence of 10 eq. [LutH]OTf/Lutidine (1 mM in THF, 0.1 M N^{n}Bu$_4$PF$_6$) at varied scan rate. * Isolated yield.

configuration was computed exergonic by ΔG°_{DFT} = 2.9 kcal mol^{-1}.

The irreversible $Re^{IV/III}$ redox couple was examined by chemical reduction of $\mathbf{3}^{\mathbf{BArF}}$ with $CoCp^*_2$ (2 eq.). Two-electron reduction is associated with a substantial structural reorganization. Bromide loss, *ortho*-metalation, tautomerization and κ*N*-to-κ*O* isomerization gives diamagnetic [Re^{III}-{$C_6H_4C(O)NH_2$}Br(PNP)] (**5**; Scheme 4) in 68 % isolated yield. Bromide ion dissociation after the second reduction is probably a prerequisite to cyclometalation. Conceivable pathways to cyclometallation are C–H oxidative addition to rhenium(III) or addition across the Re=NBz bond.[22b,24] Protonolysis of **5** with diphenyl ammonium bromide (pK_a^{THF} = 0.6)[25] restores parent **1b** and gives free benzamide in over 70 % yield (Scheme 4, top), closing a synthetic cycle from N_2 to benzamide, yet at high overpotential.

The electrochemical data of $\mathbf{3}^{+}$ reveals a remarkable anodic shift of the first reduction potential ($E_{1/2}$ = −0.71 V) with respect to parent nitride **2b** (ΔE > 2.2 V). For comparison, much smaller effects were reported for borylation of a Mo^{IV} nitride ($\Delta E \approx 350$ mV)[10] or alkylation of a Mo^{VI} nitride ($\Delta E \approx 1$ V),[26] respectively. The benzoyl-induced potential shift of $\mathbf{3}^{+}$/**4** becomes apparent upon comparison with the respective parent imide [$Re(NH)Br_2$-(^{H}PNP)]$^{+/0}$ ($\mathbf{8}^{+}$/**7**). For this purpose, the thermochemistry of electron cross transfer of the Re^{V}/Re^{IV} pairs $\mathbf{3}^{+}$/**4** and $\mathbf{8}^{+}$/**7** was calculated as an isodesmic reaction to avoid difficulties for computing absolute potentials (Scheme 5).[27] The reaction free energy ($\Delta_r G^{\circ}$ = −17.9 kcal mol^{-1}) indicates that the reduction of the parent rhenium(V) imide should be around 0.8 V more negative ($E_{1/2}(\mathbf{8}^{+}/\mathbf{7}) \approx -1.5$ V) than the benzoylimide *trans*-$\mathbf{3}^{+}$ ($E_{1/2}$ = −0.71 V). The computations further confirm a low N–H bond strength of the parent rhenium(IV) imide *trans*-**7** ($BDFE_{N-H}$ = 33.2 kcal mol^{-1}),[28] which is very close to that of the related complex [Re(NH)Cl{N-($CH_2CH_2PtBu_2$)$_2$}] (Scheme 1), rendering **7** thermodynamically unstable with respect to hydrogen evolution ($BDFE_{H-H}$ = 52 kcal mol^{-1} in THF).[29] Furthermore, as judged from a thermochemical cycle, the protonation of **2b** requires strong acids (pK_a^{THF}(*trans*-$\mathbf{8}^{+}$) ≈ 5).

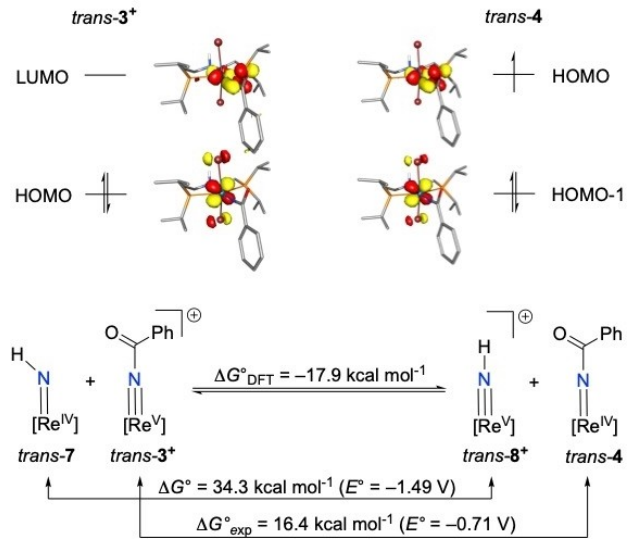

Scheme 5. Top: Frontier Kohn–Sham MOs of *trans*-$\mathbf{3}^{+}$ (left) and *cis*-**4** (right). Bottom: Thermochemistry of electron cross equilibrium of *trans*-$\mathbf{3}^{+}$/**4** with *trans*-**7**/$\mathbf{8}^{+}$. For simplicity, the *trans*-configurations were used for all states. Note that the *cis*-configuration is slightly more stable for **4** (ΔG = 2.9 kcal mol^{-1}). See Supporting Information for the *cis*-isomers.

The thermochemical bias in favour of benzoyl- vs. proton-coupled reduction can be rationalized by π-bonding within the {Re≡N–R} core (R = Bz, H). While the Re^{V} imides $\mathbf{3}^{+}$ and $\mathbf{8}^{+}$ as well as the Re^{IV} imide **4** are nearly linear, **7** was computed to be distinctly bent (∠Re–N–H: 120°). This conformational reorganization can be attributed to population of a molecular orbital (MO) with π^*_{Re-N} character. Bending of the Re–N–H moiety reduces the 3-electron interaction of the d_{Re} and p_N atomic orbitals. In contrast to hydrogen, the benzoyl substituent is a moderate π-acceptor. In fact, Nielson et al. previously described the acylimido ligand $(NC(O)H)^{2-}$ as a single faced π-donor.[30] The population of a molecular orbital with {Re≡NBz} π* character in **4** (Scheme 5) is in line with the significant elongation of the Re–N bond with respect to $\mathbf{3}^{+}$ (see above). In turn, π_{N-C} and π^*_{C-O} character of the SOMO of **4** leads to contraction of the N–C (Δd = 0.08 Å) and elongation of the C–O (Δd = 0.07 Å) bonds. Hence, charge delocalization into the benzoyl substituent contributes to the remarkable anodic shift of the reduction potential with respect to the nitride and parent imide complexes.

This thermochemical framework emphasizes that ammonia formation will be hampered by the unfavourable first PCET to **2b**. We therefore aimed at utilizing the preference in favour of Bz^{+}/e^{-} transfer to control the selectivity of nitride transfer. Full release of organic products requires further reduction and addition of electrophiles. For this purpose, PCET of the benzoylimido complex was examined. Addition of 2,6-dichlorphenol (11 eq.; pK_a^{THF} = 25.1)[31] to $\mathbf{3}^{\mathbf{BArF}}$ leads to a significant anodic shift of the irreversible, second reduction by around +400 mV, suggesting PCET (Figure S63). In the presence of the stronger acid lutidinium triflate ([LutH]OTf; 10 eq.; pK_a^{THF} = 7.2),[32] the first wave retains the reversible reduction, yet with anodically shifted potential ($E_{1/2}$ = −0.66 V; ΔE = 50 mV) and significantly higher peak current, supporting a multi-electron process (Scheme 4). Accordingly, chemical reduction of $\mathbf{3}^{\mathbf{BArF}}$ with $CoCp_2$ and lutidinium bromide (2 eq. each) gives rhenium(III) carboxamide complex **6** in 87 % spectroscopic yield (Scheme 4) and traces of **1b** (3 %). Crystallographic characterization of **6** confirms single bond character of the Re–NHBz bond (d_{Re1-N2} = 2.113(4) Å) after $2e^{-}/H^{+}$ reduction (Figure 1). The full, chemically driven nitrogen transfer can be obtained upon addition of the strong acid [Ph_2NH_2]Br (pK_a^{THF} = 0.6),[25] giving free benzamide and **1b** in yields of 56 % and 80 %, respectively (Scheme 4).

Motivated by these results, we developed protocols for direct, one-pot (electro-)chemically driven nitride transfer from **2b**. Addition of benzoyl bromide (3 eq.), [LutH]BAr^{F}_{24} (3 eq.), and the mild chemical reductant $FeCp^*_2$ (3 eq.; $E_{1/2}$ = −0.43 V)[33] to **2b** in THF-d_8 (Scheme 6, Entry 1 and Figure S74) gives parent **1b** as the only detectable product

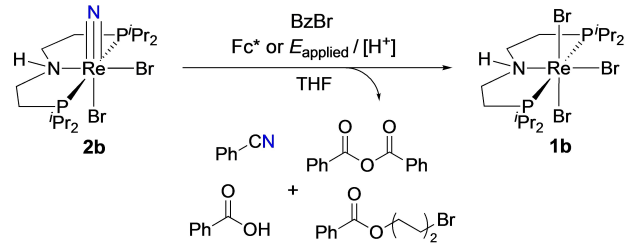

Entry	PCET reagents	Yields (FE)				
	reductant or E_{appl} / [H+]	[Re]	PhCN	Bz_2O	BzOH	$BzO(CH_2)_4Br$
1	Fc* / [LutH]BAr^F_{24}	55% (**1b**)	56%	43%	23%	26%
2	Fc* / [Et_3NH]BAr^F_{24}	82% (**1b**)	77%	78%	17%	84%
3	Fc* (without acid)	9% (**9**)	10%	<1%	58%	60%
4	-0.68 V / [LutH]BAr^F_{24} (1.62 e^- / Re)	66% (**1b**) (81%)	51% (63%)	18%	57%[a]	117%
5	-0.74 V / [Et_3NH]BAr^F_{24} (1.88 e^- / Re)	69% (**1b**) (73%)	66% (70%)	47%	-	133%

Scheme 6. Reaction conditions for one-pot (electro-)chemical nitride transfer from N_2 derived nitride **2b** to give **1b** and benzonitrile. All yields refer to rhenium nitride complex **2b**; FE = Faradaic Efficiency. [a] The yield in BzOH defines an upper limit; it was indirectly estimated by ^{1}H-NMR spectroscopy from integration of the signals of BzO-$(CH_2)_4$Br, which are superimposed with those of BzOH (see Supporting Information pp. S54–S58).

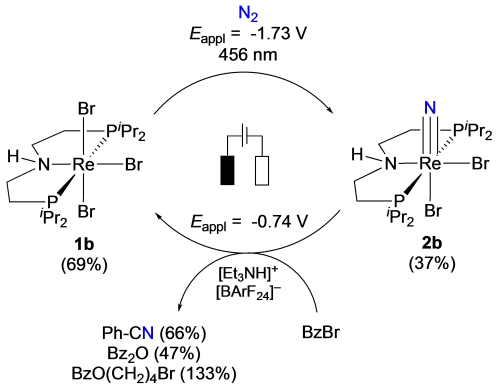

Scheme 7. 2-Step photoelectrosynthetic cycle for the conversion of N_2 to benzonitrile at ambient conditions.

by ^{31}P NMR spectroscopy in 55 % yield, together with an equimolar amount of benzonitrile (56 %). The use of the ^{15}N labelled nitride complex from photoelectrochemical splitting of $^{15}N_2$ confirmed nitride transfer to the organic product (Figure S76). Ammonium as a potential product is not detected. Besides PhCN, benzoyl anhydride (43 %) and benzoic acid (23 %) are observed. This is in line with initial formation of benzamide, which subsequently reacts with additional BzBr to benzonitrile and the anhydride/acid.[34] The formation of some 4-bromobutyl benzoate (26 %) is attributed to electrophilic ring opening of THF with benzoyl bromide, which is catalysed by Lewis acids.[35] Increased yields for both benzonitrile (77 %) and **1b** (82 %) are obtained with the weaker acid [Et_3NH]BAr^F_{24} (Scheme 6, Entry 2). Without additional acid, benzonitrile yields are strongly reduced (10 %; Scheme 6, Entry 3). Furthermore, instead of **1b** the rhenium(III) imine complex [$ReBr_3${N-$(CHCH_2P^iPr_2)(CH_2CH_2P^iPr_2)$}] (**9**) is spectroscopically observed in 9 % yield as the only identified rhenium product upon comparison with an original sample. Complex **9** is most conveniently obtained from reaction of **1** with 2,4,6-tri-*tert*-butylphenoxyl radical and was fully characterized including X-ray crystallography.[15] The dehydrogenation of the PNP ligand during reductive nitride transfer underlines the necessity of acid for full nitrogen release, presumably via PCET after *N*-benzoylation.

One-pot electrochemical nitride transfer is accomplished upon CPE of **2b** at the potential of the first reduction (E_{app} = −0.68 V) in the presence of BzBr (5 eq.) and [LutH]BAr^F_{24} (3 eq.) for 22 h (Scheme 6, Entry 4). Similar yields in benzonitrile (51 %; FE = 63 %) and **1b** (66 %; FE = 81 %) could be obtained compared to chemical reduction (Scheme 6, Entry 1). The spectroscopic yield in **1b** is in line with the transfer of 1.62e^- per Re during electrolysis. With [Et_3NH]BAr^F_{24} (Scheme 6, Entry 5), slightly increased yields in benzonitrile (66 %; FE = 70 %) and **1b** (69 %; FE = 73 %) are obtained, whereas 1.88e^- per Re are transferred. For the electrochemical protocols, slightly higher amounts of BzBr (5 eq.) are required to compensate for an increased formation of the side product from THF ring opening, 4-bromobutyl benzoate (117 % and 133 %), as compared with the use of chemical reductants. A control electrolysis experiment without **2b** confirmed the absence of PhCN, Bz_2O, and BzOH, yet indicated formation of the THF ring-opening product. The electrochemical protocol closes a 2-step electrosynthetic cycle for benzonitrile generation from N_2 after photoelectrochemical N_2 splitting (Scheme 7).

Conclusion

In summary, we have demonstrated a two-step photoelectrochemical cycle for the fixation of dinitrogen with benzoyl bromide to yield benzonitrile. Moving to the higher halide precursors significantly shifts both reductive N_2 activation to less negative potentials and photolytic N–N splitting deeper into the visible range. The unfavourable first PCET step renders the resulting nitride (X = Br) unsuitable for efficient ammonia generation. PCET cannot compete with benzoylation/reduction, which can at least in part be attributed to π-stabilization of the unusual rhenium(IV) imido state by the benzoyl substituent. This thermochemical bias provides a PCET-based, conceptual basis to enable selective, electrochemical formation of nitrogenous organic products over ammonia production. We have demonstrated this by the development of an electrochemical one-pot protocol for nitride transfer upon reduction at mild potential (E_{appl} = −0.74 V), which is compatible with the organic electrophile (BzBr) and acid (Et_3NH^+), to restore parent **1b**. The release of benzonitrile in 66 % yield is attributed to two PCET steps that follow benzoylation of the nitride with increased driving force and subsequent trapping of benzamide. Our results provide a new, PCET-based N_2 fixation

strategy for the selective formation of organic, nitrogenous products.

Acknowledgements

This work was supported by the European Research Council (ERC CoG Agreement 646747) and the German Research Council (DFG SCHN950/7, KR4848/1). All calculations were conducted on the Lichtenberg high performance computer of TU Darmstadt. The Hessian Competence Center for High Performance Computing is gratefully acknowledged. Open Access funding enabled and organized by Projekt DEAL.

Conflict of Interest

The authors declare no conflict of interest.

Data Availability Statement

The data that support the findings of this study are available from the corresponding author upon reasonable request.

Keywords: Electrochemistry · N_2 Fixation · Photochemistry · Reaction Mechanisms · Rhenium

[1] a) H. V. Huynh, T. J. Meyer, *Chem. Rev.* **2007**, *107*, 5004–5064; b) C. Costentin, M. Robert, J.-M. Savéant, *Acc. Chem. Res.* **2010**, *43*, 1019–1029; c) J. J. Warren, T. A. Tronic, J. M. Mayer, *Chem. Rev.* **2010**, *110*, 6961–7001.

[2] Y. Ashida, K. Arashiba, K. Nakajima, Y. Nishibayashi, *Nature* **2019**, *568*, 536–540.

[3] M. Chalkley, M. W. Drover, J. C. Peters, *Chem. Rev.* **2020**, *120*, 5582–5636.

[4] Q. J. Bruch, G. P. Connor, N. D. McMillion, A. S. Goldman, F. Hasanayn, P. L. Holland, A. J. M. Miller, *ACS Catal.* **2020**, *10*, 10826–10846.

[5] a) "Functionalization of N_2 by Mid to Late Transition Metals via N–N- bond cleavage": I. Klopsch, E. Y. Yuzik-Klimova, S. Schneider, in *Topics in Organometallic Chemistry, Vol. 60*, Elsevier, Amsterdam, **2017**; pp. 71–112; b) S. Forrest, B. Schluschaß, E. Yuzik-Klimova, *Chem. Rev.* **2021**, *121*, 6522–6587.

[6] a) "Determining and Understanding N–H Bond Strengths in Synthetic Nitrogen Fixation Cycles": M. J. Bezdek, I. Pappas, P. J. Chirik, in *Topics in Organometallic Chemistry, Vol. 60*, Elsevier, Amsterdam, **2017**, pp. 1–21; b) B. D. Matson, J. C. Peters, *ACS Catal.* **2018**, *8*, 1448–1455; c) Q. J. Bruch, G. P. Connor, C.-H. Chen, P. L. Holland, J. M. Mayer, F. Hasanayn, A. J. M. Miller, *J. Am. Chem. Soc.* **2019**, *141*, 20198–20208; d) G. P. Connor, D. Delony, J. E. Weber, B. Q. Mercado, J. B. Curley, S. Schneider, J. M. Mayer, P. L. Holland, *Chem. Sci.* **2022**, *13*, 4010–4018.

[7] K. Arashiba, A. Eizawa, H. Tanaka, K. Nakajima, K. Yoshizawa, Y. Nishibayashi, *Bull. Chem. Soc. Jpn.* **2017**, *90*, 1111–1118.

[8] S. Kim, Y. Park, J. Kim, T. P. Pabst, P. J. Chirik, *Nat. Synth.* **2022**, *1*, 297–303.

[9] S. Kim, F. Loose, P. J. Chirik, *Chem. Rev.* **2020**, *120*, 5637–5681.

[10] S. Bennaamane, M. Espada, A. Mulas, T. Personeni, N. Saffron-Merceron, M. Fustier-Boutignon, C. Bucher, N. Mézailles, *Angew. Chem. Int. Ed.* **2021**, *60*, 20210–20214; *Angew. Chem.* **2021**, *133*, 20372–20376.

[11] D. L. Hughes, S. K. Ibrahim, C. J. Macdonald, H. M. Ali, C. J. Pickett, *J. Chem. Soc. Chem. Commun.* **1992**, 1762–1763.

[12] H. G. Roth, N. A. Romero, D. A. Niecewicz, *Synlett* **2016**, *27*, 714–723.

[13] a) I. Klopsch, M. Finger, C. Würtele, B. Milde, D. B. Werz, S. Schneider, *J. Am. Chem. Soc.* **2014**, *136*, 6881–6883; b) I. Klopsch, M. Kinauer, M. Finger, C. Würtele, S. Schneider, *Angew. Chem. Int. Ed.* **2016**, *55*, 4786–4789; *Angew. Chem.* **2016**, *128*, 4864–4867; c) B. M. Lindley, R. S. van Alten, M. Finger, F. Schendzielorz, C. Würtele, A. J. M. Miller, I. Siewert, S. Schneider, *J. Am. Chem. Soc.* **2018**, *140*, 7922–7935; d) R. S. van Alten, F. Wätjen, S. Demeshko, A. J. M. Miller, C. Würtele, I. Siewert, S. Schneider, *Eur. J. Inorg. Chem.* **2020**, 1402–1410; e) R. A. van Alten, P. A. Wieser, M. Finger, J. Abbenseth, S. Demeshko, C. Würtele, I. Siewert, S. Schneider, *accepted*.

[14] F. Schendzielorz, M. Finger, J. Abbenseth, C. Würtele, V. Krewald, S. Schneider, *Angew. Chem. Int. Ed.* **2019**, *58*, 830–834; *Angew. Chem.* **2019**, *131*, 840–844.

[15] See Supporting Information for synthetic, spectroscopic, electrochemical, computational, and crystallographic details. Deposition Numbers 2166547 (**1b**), 2166548 (**1c**), 2166549 (**2b**), 2166550 (**2c**), 2166551 (**3^{Br}**), 2166552 (**3^{BArF}**), 2166553 (**4**), 2166554 (**5**), 2166555 (**6**), 2166556 (**9**) contain the supplementary crystallographic data for this paper. These data are provided free of charge by the joint Cambridge Crystallographic Data Centre and Fachinformationszentrum Karlsruhe Access Structures service.

[16] L. Alig, K. A. Eisenlohr, Y. Zelenkova, S. Rosendahl, R. Herbst-Irmer, S. Demeshko, M. C. Holthausen, S. Schneider, *Angew. Chem. Int. Ed.* **2022**, *61*, 202113340; *Angew. Chem.* **2022**, *134*, 202113340.

[17] All potentials are reported vs. the $[FeCp_2]^{+/0}$ reference couple.

[18] N. Salvarese, F. Refosco, R. Seraglia, M. Roverso, A. Dolmella, C. Bolzati, *Dalton Trans.* **2017**, *46*, 9180–9191.

[19] D. P. Hickey, C. Sandford, Z. Rhodes, T. Gensch, L. R. Fries, M. S. Sigman, S. D. Minteer, *J. Am. Chem. Soc.* **2019**, *141*, 1382–1392.

[20] The lower limit for chloride loss from $[\mathbf{1}^{Cl}]^-$ estimated by Bruch et al. from our previously reported data is in full agreement ($k > 0.04\ s^{-1}$; see Ref. [4]).

[21] a) M. A. Masood, B. P. Sullivan, D. J. Hodgson, *Inorg. Chem.* **1999**, *38*, 5425–5430; b) X. Schoultz, T. I. A. Gerber, R. Betz, *Inorg. Chem. Commun.* **2016**, *69*, 45–46.

[22] a) G. A. Lawrance, D. F. Sangster, *J. Chem. Soc. Chem. Commun.* **1984**, 1706–1707; b) S. N. Brown, A. W. Myers, J. R. Fulton, J. M. Mayer, *Organometallics* **1998**, *17*, 3364–3374.

[23] The lineshapes can be attributed to slow tumbling in solution: a) R. Wang, A. M. Brugh, J. Rawson, M. J. Therien, M. D. E. Forbes, *J. Am. Chem. Soc.* **2017**, *139*, 9759–9762; b) A. M. Brugh, R. Wang, M. J. Therien, M. D. E. Forbes, *ACS Omega* **2021**, *6*, 27865–27873.

[24] O. V. Ozerov, L. A. Watson, M. Pink, K. G. Caulton, *J. Am. Chem. Soc.* **2007**, *129*, 6003–6016.

[25] S. Tshepelevitsh, A. Kütt, M. Lõkov, I. Kaljurand, J. Saame, A. Heering, P. G. Plieger, R. Vianello, I. Leito, *Eur. J. Org. Chem.* **2019**, 6735–6748.

[26] a) T. Kupfer, R. R. Schrock, *J. Am. Chem. Soc.* **2009**, *131*, 12829–12837; b) T. Munisamy R R Schrock, *Dalton Trans.* **2012**, *41*, 130–137.

[27] The *trans*-isomers were used for all four states to calculate $\Delta_r G^0$. This configuration is thermodynamically favoured in all cases except for **4**.
[28] This free energy refers to the reaction *trans*-**7**→*trans*-**2b**+H. Note that the *cis*- and *trans*-isomers of **2b** were computed as almost isoenergetic. For the reaction *cis*-**7**→*cis*-**2b**+H, a $BDFE_{N-H}$ of 32.4 kcal mol^{-1} was computed. See Supporting Information for further detail.
[29] C. F. Wise, R. G. Agarwal, J. M. Mayer, *J. Am. Chem. Soc.* **2020**, *142*, 10681–10691.
[30] A. J. Nielson, P. A. Hunt, C. E. F. Rickard, P. Schwerdtfeger, *J. Chem. Soc. Dalton Trans.* **1997**, 3311–3317.
[31] D. Barrón, J. Barbosa, *Anal. Chim. Acta* **2000**, *403*, 339–347.
[32] I. Kaljurand, A. Kütt, L. Sooväli, T. Rodima, V. Mäemets, L. Leito, I. Koppel, *J. Org. Chem.* **2005**, *70*, 1019–1028.
[33] I. Noviandri, K. N. Brown, D. S. Fleming P T Gulyas, P. A. Lay, A. F. Masters, L. Phillips, *J. Phys. Chem. B* **1999**, *103*, 6713–6722.
[34] a) D. Davidson, H. Skovronek, *J. Am. Chem. Soc.* **1958**, *80*, 376–379; b) P. Spránitz, P. Sőregi, B. Botlik, M. Berta, T. Soós, *Synthesis* **2019**, *51*, 1263–1272.
[35] S. J. Coles, J. F. Costello, W. N. Draffin, M. B. Hursthouse, S. P. Paver, *Tetrahedron* **2005**, *61*, 4447–4452.

Manuscript received: April 22, 2022
Accepted manuscript online: June 17, 2022
Version of record online: July 18, 2022